Optical properties of boreal region biomass burning aerosols in central Alaska and seasonal variation of aerosol optical depth at an Arctic coastal site

T.F. Eck[1], B.N. Holben[1], J.S. Reid[2], A. Sinyuk[1], E.J. Hyer[2], N.T. O'Neill[3], G.E. Shaw[4], J.R. Vande Castle[5], F.S. Chapin[4], O. Dubovik[6], A. Smirnov[1], E. Vermote[1], J.S. Schafer[1], D. Giles[1], I. Slutsker[1], M. Sorokine[1], W.W. Newcomb[1]

[1]NASA / GSFC, Greenbelt, MD, USA

[2]Naval Research Laboratory, Monterey, CA, USA

[3]Université de Sherbrooke, Sherbrooke, Québec, Canada

[4]University of Alaska, Fairbanks, AK

[5]University of New Mexico, Albuquerque, NM

[6]CNRS Universite de Lille, Villeneuve d'Ascq CEDEX, France

Earth's land surface or ~16 million square kilometers across northern Eurasia and North America. The arctic and boreal zones currently store the globe's largest reservoir of soil carbon, at 25-35% of the total, largely in organic soil layers in the permafrost [*Bonan and Shugart*, 1989; *Melillo et al.* 1995]. Both climate change simulations of the effects of increasing atmospheric greenhouse gas concentrations and recent observations show that global temperature increases are the largest in the arctic and boreal regions [*Soja et al.*, 2007; *IPCC*, 2007]. As a result of these temperature increases (and drier conditions) models predict future increases in area burned in the boreal zone. For example *Flannigan et al.* [2005] simulated a 74-118% increase in burned area in Canada by 2100 in a $3XCO_2$ increase scenario. *Kharuk et al.* [2008] found a one-third reduction in fire return interval time for larch dominated forests in Siberia from the 19th to the 20th century, related to warming temperatures in northeast Siberia. Severe forest fires that also burn insulating organic and peat soil layers result in deeper soil thawing [*Kharuk et al.*, 2008] and thereby may release large amounts of stored carbon into the atmosphere.

Concurrent with a significant warming trend, *Kasischke and Turetsky* [2006] found that the annual boreal forest area burned in Alaska and Canada doubled from the 1960s/70s to the 80s/90s and the proportion of burning in the early and late growing seasons increased. In Alaska seven of the eleven largest fires in a 56 year interval (1950-2005) have burned since 1988, with the largest area burned on record occurring in 2004 and the third largest in 2005 [*Soja et al.*, 2007]. Across the entire circumboreal zone the frequency of extreme fire years has increased. *Kasischke et al.* [2002] have found that high fire years in Alaska consist of larger fires occurring later in the growing season. In low precipitation years peat burning is expected to increase as the summer advances due

70 strong boreal burning years they attribute ~80% of the global BC/snow forcing to be from
71 anthropogenic fossil fuel and biofuel sources.

72 Only recently have studies investigated the optical properties of boreal region biomass
73 burning aerosols in intensive burning years [*Stohl et al.*, 2006b; *Myhre et al.*, 2007].
74 *Pfister et al.* [2008] discuss the need for better characterization of the optical properties
75 of boreal region biomass burning smoke particles, especially for the case of significant
76 peat burning. In this investigation we present an analysis of a long time series of aerosol
77 optical depth measurements from 1994 through 2008 at an AERONET sun-sky
78 radiometer site located in the boreal forest zone of central Alaska. In the extreme burning
79 years of 2004 and 2005 the AOD was very high, allowing for accurate characterization of
80 the spectral imaginary refractive index (absorption) and single scattering albedo (ω_0)
81 from almucantar retrievals. Additionally, we compare the particle size distributions and
82 ω_0 of these fine mode dominated smoke aerosols to the size distributions and absorption
83 of smoke aerosols from other major biomass burning regions. We also present AOD data
84 from a site on the Arctic Ocean coast in Alaska to compare the seasonality and frequency
85 of smoke transport to the Arctic (primarily in summer) to the springtime Arctic haze
86 impacts on optical depth. The Arctic haze phenomenon has been attributed primarily to
87 the long-distance transport of aerosols from industrial source regions (Shaw, 1995).
88

89 **2. Instrumentation, Study Sites and Techniques**

90 **2.1 Study Region and Sites**

91 The principal AERONET site analyzed in this study is the Bonanza Creek, Alaska site
92 located in the boreal forest biome of central Alaska (Figure **1**). This is a National Science

every 15 minutes at 340, 380, 440, 500, 675, 870, 940, and 1020 nm (nominal wavelengths). The direct sun measurements take ~8 seconds to scan all 8 wavelengths, with a motor driven filter wheel positioning each filter in front of the detector. These solar extinction measurements are then used to compute aerosol optical depth (AOD, τ_a) at each wavelength except for the 940 nm channel, which is used to retrieve total columnar (or precipitable) water vapor in centimeters. The filters utilized in these instruments were ion assisted deposition interference filters with bandpass (full width at half maximum) of 10 nm, except for the 340 and 380 nm channels at 2 nm. The estimated uncertainty in computed τ_a, due primarily to calibration uncertainty, is ~0.010-0.021 for field instruments (which is spectrally dependent with the higher errors in the UV; *Eck et al.* [1999]). *Schmid et al.* [1999] compared τ_a values derived from 4 different solar radiometers (including an AERONET sun-sky radiometer) operating simultaneously together in a field experiment and found that the τ_a values from 380 to 1020 nm agreed to within 0.015 (rms), which is similar to our estimated level of uncertainty in τ_a retrieval for field instruments. The spectral aerosol optical depth data have been screened for clouds following the methodology of *Smirnov et al.* [2000], which relies on the greater temporal variance of cloud optical depth versus aerosol optical depth. The sky radiances measured by the sun/sky radiometers are calibrated versus the 2-meter integrating sphere at the NASA Goddard Space Flight Center, to an absolute accuracy of ~5% or better.

2.3 Inversion Methodology

161 to demonstrate successful retrievals of mode radii and the relative magnitude of modes
162 for various types of bimodal size distributions such as those dominated by a sub-micron
163 accumulation mode or distributions dominated by super-micron coarse mode aerosols. To
164 ensure sufficient sensitivity to aerosol absorption, only almucantar scans where
165 AOD(440nm)>0.4 [*Dubovik et al.*, 2000] were analyzed for the investigation of the
166 characteristics of spectral refractive indices and single scattering albedo.
167

168 **3. Results and Discussion**

169 **3.1 Temporal and Spectral Variability of AOD in central Alaska**

170 **3.1.1 Monthly and inter-annual variation in AOD and Angstrom exponent**

171 The monthly climatology of 500 nm AOD and Angstrom Exponent (440-870 nm) at
172 Bonanza Creek, Alaska showing monthly means from multiple years of observations is
173 shown in Figure **2**. The 440-870 nm Angstrom is computed from linear regression of ln
174 AOD versus ln λ scale at 440, 500, 670 and 870 nm. The multi-year monthly means are
175 computed as a mean of the individual monthly averages. The seasonal trend in monthly
176 average AOD shows a steady increase of AOD from near background levels in March
177 (~0.06) to values exceeding ~0.14 for June, July and August and then a rapid 2-month
178 decline down to background again (~0.05) in October. It should be noted that the inter-
179 annual variability in AOD is extremely large (see Figure **3**, discussed below) due to the
180 episodic nature of boreal fires with severe and numerous fires occurring in drought years,
181 compared to few fires in wet years. Fine mode biomass burning aerosols dominate this
182 seasonality as the Angstrom exponent increases in summer (June-August) when most
183 burning occurs.

207 and 2008. However, in 2004 there were similar number of fires in July as August while
208 the AOD at Bonanza Creek was >2.5 times higher in August. Daily area burned estimates
209 for Alaska and Canada combined as shown by *Stohl et al.* [2006] reach a maximum from
210 late June through July, and much less area burned in August. This suggests the possibility
211 that factors other than area burned and numbers of fires are important in determining the
212 total atmospheric column AOD. Other factors in addition to area burned that would
213 influence the AOD are meteorological conditions (including wind speed and direction,
214 atmospheric stability, and precipitation), intensity of burning since intense fires enhance
215 convection that may loft smoke to higher altitudes where winds are higher, and the types
216 of fuel burned and the phase of combustion [*Reid et al.*, 2005b]. It is noted that AOD
217 measurements at a point location (Bonanza Creek) are also strongly affected by the
218 location of the fires in the entire state of Alaska relative to the wind direction and other
219 meteorological factors. Satellite hot spot remote sensing robustly detects fires in the high
220 temperature flaming phase of combustion but it is much more difficult to detect lower
221 temperature smoldering phase fires. However the flaming phase is typically of relatively
222 short duration, while the larger diameter woody fuels in a forest and the organic soils and
223 peatlands may burn for several days in the smoldering phase. As previously mentioned,
224 *Turquety et al.* [2007] estimated that the proportion of carbon monoxide emissions was
225 double the proportion of peat area burned (~37% of the carbon monoxide emissions from
226 only 17% of the area burned) in 2004 for fires in Alaska and Canada. This suggests that
227 peat burning may possibly also have resulted in a disproportionate amount of total
228 aerosol emissions, relative to the total area burned.

variation in source strength and due to the transport, stagnation, and removal effects of regional meteorology.

Based on the assumption that aerosol size distributions are bimodal, *O'Neill et al.* (2001, 2003) have developed a spectral deconvolution algorithm (SDA) that utilizes spectral total extinction AOD data to infer the component fine and coarse mode optical depths. An additional fundamental assumption of the algorithm is that the coarse mode Angstrom exponent and its derivative are both close to zero. The Angstrom exponent α and the spectral variation of α (as parameterized by $\alpha'=d\alpha/d\ln\lambda$) are the measurement inputs to the SDA. These continuous-function derivatives (usually computed at a reference wavelength of 500 nm) are derived from a second order fit of $\ln \tau_a$ versus $\ln \lambda$ (*Eck et al.*, 1999). The spectral AODs employed as input to the SDA were limited to the six CIMEL wavelengths ranging from 380 to 1020 nm. Figure **6** shows the time series of fine and coarse mode daily average AOD at 500 nm from the SDA algorithm for June 1 through September 12, 2004 at Bonanza Creek. These are level 2 cloud screened data that have had the SDA algorithm applied to the AOD spectra. It is noted that the coarse mode is typically very low and nearly constant, while the fine mode AOD from biomass burning exhibits very large day-to-day variability. Only 2 days show the coarse mode AOD to be significantly higher than the fine mode, possibly due to dust transported from Asia or from residual cloud contamination. We assume that the fine mode aerosols at Bonanza Creek are dominated by biomass burning smoke since there are numerous fire hot spots observed (Figure 1), combined with a lack of any other significant regional sources of fine mode particles.

295 The SDA algorithm computed daily average fine mode fractions (FMF) for the
296 Bonanza Creek site are plotted versus $\alpha_{380\text{-}500}$ in Figure **8**, and compared with
297 measurements made in Brazil and Zambia (from the same observations as shown in
298 Figure **7**). For the same range of FMF, 0.8 – 1.0, the $\alpha_{380\text{-}500}$ is typically significantly
299 lower for the Alaska site than the Brazil and Zambia biomass burning sites, again
300 suggesting much larger accumulation mode particles in Alaska. In addition to the greater
301 percentage of smoldering combustion for the forest regions with woody fuels (Alaska and
302 Brazil) other possible reasons for larger accumulation mode particles include higher
303 AOD levels (Figure **7**) in Alaska and Brazil that increase the coagulation rate since
304 aerosol concentrations are higher. Another possible factor in creating large accumulation
305 particles might be the characteristics of smoke from peat burning in Alaska [*Reid et al.*,
306 2005a], since extensive areas of peat lands (in addition for forests) were observed to burn
307 during the summer of 2004.
308
309 **3.2 Retrievals of aerosol size distribution and single scattering albedo in central**
310 **Alaska**
311 **3.2.1 Volume size distributions**
312 The almucantar retrievals of aerosol volume size distributions for the Bonanza Creek
313 site in 2004 and 2005 for scans where AOD(440nm)>0.4 are shown in Figure **9a**. These
314 averages are plotted as a function of AOD(440nm) with AOD bins from 0.4-0.8, >0.8-
315 1.0,…,>2.4-2.8, >2.8 resulting in averages of from 9 to 34 almucantars per bin. At all
316 AOD levels the retrievals show the dominance of fine mode aerosols, and the $\alpha_{440\text{-}870}$ for
317 the bins range from 1.74 at the lowest AOD(440) average of 0.53 to 1.36 at the highest

341 exhibiting r_v ~ 0.21 μm and transported smoke from a Russian peat/forest fire showing
342 retrieved r_v of 0.28 μm (Version 2 retrievals as compared to somewhat smaller radius
343 values reported from Version 1 in *Eck et al.* [2003a]). These however were aged aerosol
344 events with smoke age > 2 days due to long distance transport from distinct source
345 regions. However, AERONET measurements made in Moscow on September 7, 2002
346 (AOD(440) ~2.5) near to a fire that was predominately burning peat had large
347 accumulation mode particles of ~0.22 μm radius despite relatively short transport
348 distance and therefore likely little aging. Therefore, the large radius of the smoke aerosol
349 measured in late summer in Alaska in 2004 and 2005 possibly resulted in part from the
350 smoldering combustion of peat fuels in addition to the high aerosol concentrations that
351 would result in greater coagulation, condensation and secondary production rates.
352 In comparison to the Alaska smoke we show the aerosol volume size distribution
353 retrievals for biomass burning aerosols from the Mongu, Zambia AERONET site in
354 Figure **11a**. These retrievals are from September (peak burning month) data only for the
355 years 1997-2005, and shown for two AOD levels, ~0.5 and ~1.3 at 440 nm. Both the
356 mean sizes and the shift of fine mode radius as AOD increases in Zambia are relatively
357 small (radius ~0.14 to 0.16 μm) as compared to the boreal smoke measured in Alaska.
358 Smoke in Brazil (southern Amazonia; not shown) exhibited slightly larger fine mode
359 radius (~0.15 to 0.17 μm; *Schafer et al.*, 2008) at these AOD levels than Zambia, possibly
360 due to more smoldering combustion of woody fuels and higher aerosol concentrations
361 that may have lead to greater coagulation rates. In addition to the relatively small change
362 in volume median radius in Mongu, Zambia, the width of the fine mode size distribution
363 is narrower for the Zambia smoke than for the Alaska smoke. The geometric standard

386 The average single scattering albedo in 2004 and 2005 at Bonanza Creek is high
387 (weak absorption) for biomass burning aerosols, with most values ranging from ~0.96 to
388 0.97 (Figure **9b**). Only four of the individual retrievals out of a total of 124 almucantars
389 with AOD(440nm)>0.4 in 2004 and 2005 had ω_0 less than 0.935 at 440 nm, with the
390 lowest at 0.909. The highest retrieved value of ω_0 at 440 nm was 0.996. For all but the
391 lowest AOD level the average ω_0 at 440 nm is slightly lower (by ~0.01) than that at 675
392 nm, and the ω_0 from 675 nm through 1020 nm are relatively constant (Figure **9b**). This
393 spectral dependence of ω_0 appears to be anomalous for biomass burning aerosols, as the
394 single scattering albedo typically decreases with increasing wavelength in both
395 measurements and retrievals [*Reid et al.*, 2005b]. For example, *Dubovik et al.* [2002]
396 show this typical wavelength dependence for biomass burning aerosols from four major
397 regions: Amazonian forest, S. American cerrado (savanna-like), African savanna in
398 Zambia, and boreal forest (primarily Canada). However, the boreal forest data set in
399 *Dubovik et al.* [2002] does not include events with as high AOD as occurred in Alaska in
400 2004 and 2005, nor does it include observations with significant peat burning. For all
401 other years from 1994-2007 (excluding 2004 and 2005) there were a total of only 14
402 almucantar retrievals at Bonanza Creek with AOD(440nm)>0.4. Two of these had ω_0 at
403 400 nm of ~0.86 which suggests flaming phase crown fires, while the other 12 had values
404 ranging from 0.92 to 0.98. The mean of these 14 almucantars was 0.94 at 440 nm and
405 within less than 0.005 of the values given by *Dubovik et al.* [2002] at all 4 wavelengths
406 (Dubovik's values were a mean for boreal forest biomass burning aerosols).
407 Similar wavelength dependence of ω_0 to the Alaskan smoke of 2004 and 2005 was
408 observed however for the previous mentioned case of peat burning smoke in Moscow on

higher and relatively constant (~0.72). For the burning of lignite fuel *Bond et al.* [1999] also measured greater fine particle absorption at shorter wavelengths (450 nm), implying larger imaginary refractive index at shorter wavelengths, possibly due to absorption by organic carbon. It is noted that their laboratory combustion of this lignite fuel occurred partially in the smoldering phase. However it is noted that the absorption properties of organic carbon are not well known and therefore are a topic of much recent research.

Another factor that contributes to the relatively constant spectral single scattering albedo of the Alaskan smoke is the much larger size and wider distribution of the fine mode particle radius, as compared to particles from most other biomass burning regions. Because the scattering cross section (or hence scattering optical depth) increases more rapidly than absorption cross section with increasing particle size the SSA also increases (in the absence of variations in refractive index) with increasing particle size. This trend is the optical equivalent of stating (as above) that SSA typically decreases with increasing wavelength. However this trend is less extreme at larger particle sizes because the SSA approaches unity at a lesser rate with respect to increasing particle size (or decreasing wavelength).

In situ measurements from nephelometer and particle soot absorption photometer data at the surface in Barrow, Alaska on July 3-4, 2004 yielded an aerosol single scattering albedo of 0.96 at 550 nm [*Stohl et al.*, 2006; *Stone et al.*, 2008], for a case of very high smoke AOD advected from fires in central Alaska and the Yukon. This is essentially equal to the mean AERONET retrievals of ω_0 interpolated to 550 nm for the total column aerosol in central Alaska at Bonanza Creek (Figure 9a). For agricultural smoke originating in Europe and subsequently advected to Svalbard in the Arctic, *Myhre et al.*

478 conditions, *Lewis et al.* [2008] measured AAE as high as 2.5 (532 to 870 nm) at high ω_0
479 (near unity) while AAE values approached 1.0 for $\omega_0 < 0.8$ at 532nm. The measured
480 organic carbon fraction to total carbon was highest for the smoke with the highest AAE
481 and ω_0, thereby suggesting that the enhanced absorption AAE results from light
482 absorbing organic carbon.
483
484 **3.3 Seasonal variation of AOD in the coastal Arctic at Barrow, Alaska**
485 In this section we present data from the Arctic AERONET site located at Barrow,
486 Alaska on the Beaufort Sea coast (Figure 1). The data collection at this site has many
487 more gaps than for the Bonanza Creek site in central Alaska due to its more severe
488 weather, which sometimes resulted in instrument electronic or mechanical problems. This
489 occurred especially in earlier years before a modified version of the CIMEL that
490 incorporated heating elements was deployed. Additionally there is more persistent cloud
491 cover at this site than at Bonanza Creek, resulting in fewer observations of the sun,
492 therefore less AOD measurements and very few almucantar scans of sky radiance
493 distribution. Data were acquired in 1999, 2002, 2004, 2005, 2006, 2007, and 2008
494 however measurements were only made during the peak Arctic haze month of April in
495 three years, 2002, 2005 and 2008, when data collection began in late March or early
496 April. All years had monitoring from July through September, and four of the six years
497 had data from May through September, thus covering the biomass burning season.
498 Therefore due to the numerous gaps in data acquisition, the AERONET data presented
499 here for Barrow cannot be considered a fully representative monitoring record, especially
500 for the spring arctic haze season. These data gaps therefore preclude any analysis of

524 solar zenith angle. *Stohl et al.* [2006a] have shown from transport modeling that this
525 smoke event originated from the fires located in central Alaska and the Canadian Yukon,
526 and that the smoke continued to be transported beyond Barrow and deep into the arctic.
527 Their simulations suggested that smoke from this event reached the North Pole on July 8,
528 2004 although cloud cover precluded verification from satellite images. The AERONET
529 site located at Resolute Bay, Canada (74^0 44' N, 94^0 54' W; ~1950 km ENE from
530 Barrow) measured smoke AOD on July 5, 2004 as high as 2.3 at 500 nm ($\alpha_{440\text{-}870} > 1.3$)
531 from this same arctic transport event. A Terra MODIS image (Figure 7 in Stohl et al.
532 (2006)) shows widespread smoke from Alaska and the Yukon through the Arctic islands
533 of Canada on July 5, 2004.

534 Figure **12**b is the same as **12**a but with the extreme AOD event of July 3, 2004
535 excluded. Individual daily averages of AOD are shown as well as 20 day interval means
536 (means computed with the one extreme day removed also). Seasonality of AOD is
537 evident, with the highest 20-day averages of AOD occurring during the arctic haze season
538 from late March through mid-May. These higher average AOD values result partly from
539 the lack of measured low background AOD in the spring, when values are rarely lower
540 than 0.07. In contrast the daily average AOD during summer months is often <0.04 and
541 as low as 0.02. However daily average AOD on some summer days, as high as or higher
542 than the spring Arctic haze AOD, from biomass burning aerosols result in mean values of
543 AOD during the summer that are elevated significantly above background levels. Again it
544 is emphasized that due to a much less extensive data record at Barrow (as compared to
545 Bonanza Creek), and since the extreme Alaska burning years of 2004 and 2005 are

569 monthly average Angstrom Exponent (440-870 nm) at both sites, 1.25 at Barrow and 1.10
570 at Bonanza Creek.

571 *Shaw* [1982] measured AOD from sunphotometer at Barrow during the mid to late
572 1970s and computed a March-April mean of 0.135 at 500 nm. Therefore the mean AOD
573 measured by AERONET for the spring arctic haze (and smoke) at Barrow for 2002, 2005
574 and 2008 were somewhat higher than that measured ~25 years earlier. *Bodhaine and*
575 *Dutton* [1993] presented measurements of AOD at Barrow computed from broadband
576 (300-690 nm) pyrheliometer measurements for the years 1977-1992, with estimates of
577 volcanic aerosol optical depth removed. They show relatively low AOD in 1980 and
578 1981 and a significant downward trend from 1982 (peak year) to 1992 that they suggest
579 may have resulted from the reduction of emissions in the Soviet Union and Europe during
580 that era. Continued monitoring of AOD at Barrow is important for understanding arctic
581 haze magnitude and trends. Ground based photometric measurements of AOD at 532 nm
582 at the arctic island of Spitsbergen (~79N, 12E) by *Herber et al.* [2002] from 1991
583 through 1999 showed a gradual increase in AOD of ~9% over the 9 year interval. The
584 relative sparseness of long-term records of AOD at Arctic locations coupled with the
585 possibility of different regional influences (sources and meteorology) make it very
586 difficult to assess trends of aerosol loading across the entire arctic region.
587

588 **4. Summary and Conclusions**

589

590 Aerosol optical properties data acquired from monitoring at two AERONET sites in
591 Alaska were investigated. Data from long-term monitoring at a central Alaska boreal

3. Absorption by the smoke aerosol in Bonanza Creek in 2004 and 2005 was very weak, with retrieved single scattering albedo ranging from ~0.96 to 0.97, along with relatively flat spectral dependence. These high single scattering albedos result from small values of the imaginary index of refraction, implying low black carbon fraction probably due to predominately smoldering combustion, coupled with large fine mode particle radius which results in greater scattering efficiency (increased ω_o amplitude) and reduced wavelength dependence of the ω_o. Additionally, the single scattering albedo at 440 nm was ~0.01 lower than at the longer wavelengths due to a somewhat larger imaginary refractive index at 440 nm, which is possibly due to enhanced short wavelength absorption by organic carbon aerosols. This also suggests the possibility that smoke from peat burning (smoldering combustion) had a significant influence on aerosol emissions.
4. Although AERONET monitoring at the Arctic coastal site of Barrow from 1999 to 2008 was often interrupted and not complete enough to be considered a representative climatology, some seasonal characteristics of AOD were nonetheless evident. The average AOD in the spring (late March through late May) is higher than the average AOD in the summer. Even though several individual daily mean values in summer are significantly higher (from transported biomass burning smoke) than most daily means in spring, the lack of very low background AOD levels in spring, due primarily to persistent industrial arctic haze, resulted in higher mean AOD in spring.

Acknowledgements

658 Bergstrom, R.W., P. Pilewskie, P. B. Russell, J. Redemann, T. C. Bond, P. K. Quinn, and
659 B. Sierau, Spectral absorption properties of atmospheric aerosols, Atmos. Chem. Phys.,
660 7, 5937–5943, 2007.
661 Bodhaine, B.A. and E.G. Dutton, A Long-Term Decrease In Arctic Haze At Barrow,
662 Alaska, Geophys. Res. Lett., 20 (10), 947-950, 1993.
663 Bonan, G.B. and H.H. Shugart (1989), Environmental factors and ecological processes in
664 boreal forests. *Annual Review of Ecology and Systematics*, 20, 1-28.
665 Bond, T. C., Anderson, T. L., and Campbell, D.: Calibration and intercomparison of
666 filter-based measurements of visible light absorption by aerosols, Aero. Sci. Technol.,
667 30, 582–600, 1999.
668 Dubovik, O., A. Smirnov, B. N. Holben, M. D. King, Y. J. Kaufman, T. F. Eck, and I.
669 Slutsker, Accuracy assessments of aerosol optical properties retrieved from AERONET
670 Sun and sky-radiance measurements, J. Geophys. Res.,105, 9791-9806, 2000.
671 Dubovik, O. and M.D. King, A flexible inversion algorithm for the retrieval of aerosol
672 optical properties from Sun and sky radiance measurements, J. Geophys. Res.,105,
673 20673-20696, 2000.
674 Dubovik, O., B.N. Holben, T.F. Eck, A. Smirnov, Y.J. Kaufman, M.D. King, D. Tanre, I.
675 Slutsker, Variability of absorption and optical properties of key aerosol types observed
676 in worldwide locations, J. Atmos. Sci., 59, 590-608, 2002.
677 Dubovik, O. et al., 2006: Application of spheroid models to account for aerosol particle
678 nonsphericity in remote sensing of desert dust. *J. Geophys. Res.*, **111**,
679 doi:10.1029/2005JD006619.
680 Eck, T.F., B.N. Holben, J.S. Reid, O. Dubovik, A. Smirnov, N.T. O'Neill, I. Slutsker, and

703 Engvall, A.-C., R. Krejci1, J. Strom, R. Treffeisen, R. Scheele, O. Hermansen, and J.
704 Paatero (2008), Changes in aerosol properties during spring-summer period in the
705 Arctic troposphere, Atmos. Chem. Phys., 8, 445–462.
706 Flanner, M. G., C. S. Zender, J. T. Randerson, and P. J. Rasch (2007), Present-day
707 climate forcing and response from black carbon in snow, *J. Geophys. Res.*, *112*,
708 D11202, doi:10.1029/2006JD008003.
709 Flannigan M.D., K.A. Logan, B.D. Amiro, W.R. Skinner, and B.J. Stocks (2005), Future
710 area burned in Canada, Climat. Change, 72, 1-16.
711 Generoso, S., I. Bey, J.-L. Attié, and F.-M. Bréon (2007), A satellite- and model-based
712 assessment of the 2003 Russian fires: Impact on the Arctic region, *J. Geophys. Res.*,
713 *112*, D15302, doi:10.1029/2006JD008344.
714 Hansen J. and L. Nazarenko, Soot climate forcing via snow and ice albedos, Proc. Nat.
715 Acad. Sci., 101 (2), 423-428, 2004.
716 Herber, A., L.W. Thomason, H. Gernandt, U. Leiterer, D. Nagel, K.H. Schulz, J. Kaptur,
717 T. Albrecht, and J. Notholt, Continuous day and night aerosol optical depth
718 observations in the Arctic between 1991 and 1999, J. Geophys. Res., 107 (D10), 4097,
719 2002.
720 Holben, B.N., T.F. Eck, I. Slutsker, A. Smirnov, A. Sinyuk, J. Schafer, D. Giles, and O.
721 Dubovik, AERONET's Version 2.0 quality assurance criteria, Remote Sensing of
722 Atmosphere and Clouds, edited by Si-Chee Tsay, T. Nakajima, R.P. Singh, and R.
723 Sridharan, Proc. SPIE Vol. 6408, 64080Q, doi:10.1117/12.706524, 2006.
724 Holben, B.N. et al., AERONET - A federated instrument network and data archive for
725 aerosol characterization, Remote Sens. Environ., 66, 1-16, 1998.

749 (1995), Global change and its effects on soil organic carbon stocks. In: Role of
750 Nonliving Organic Matter in the Earth's Carbon Cycle (eds Zepp RG, Sontaff CH), pp.
751 175-189. John Wiley, New York.
752 Myhre, C. L., C. Toledano, G. Myhre, K. Stebel, K. E. Yttri, V. Aaltonen, M. Johnsrud,
753 M. Frioud, V. Cachorro, A. de Frutos, H. Lihavainen, J. R. Campell, A. P. Chaikovsky,
754 M. Shiobara, E. J. Welton, and K. Tørseth (2007), Regional aerosol optical properties
755 and radiative impact of the extreme smoke event in the European Arctic in spring 2006,
756 Atmos. Chem. Phys., 7, 5899–5915.
757 O'Neill, N.T., T.F. Eck, B.N. Holben, A. Smirnov, O. Dubovik, and A. Royer, Bimodal
758 size distribution influences on the variation of Angstrom derivatives in spectral and
759 optical depth space, J. Geophys. Res., 106, 9787-9806, 2001.
760 O'Neill, N.T., T.F.Eck, , A.Smirnov, B.N.Holben, and S.Thulasiraman, 2003, Spectral
761 discrimination of coarse and fine mode optical deph, J. Geophys. Res., 108(D17), 4559,
762 doi:10.1029/2002JD002975.
763 Pfister, G. G., P. G. Hess, L. K. Emmons, P. J. Rasch, and F. M. Vitt (2008), Impact of
764 the summer 2004 Alaska fires on top of the atmosphere clear-sky radiation fluxes, *J.*
765 *Geophys. Res.*, *113*, D02204, doi:10.1029/2007JD008797.
766 Reid, J. S., and P. V. Hobbs (1998), Physical and optical properties of young smoke from
767 individual biomass fires in Brazil, *J. Geophys. Res.*, *103*(D24), 32,013–32,030.
768 Reid, J.S., T.F. Eck, S.A. Christopher, P.V. Hobbs, and B.N. Holben (1999), Use of the
769 Angstrom exponent to estimate the variability of optical and physical properties of
770 aging smoke particles in Brazil, J. Geophys. Res.,104, 27,473-27,489.
771 Reid, J. S., R. Koppmann, T. Eck, and D. Eleuterio (2005a), A review of biomass

795 Stocks, A. I. Sukhinin, E.I. Parfenova, F. S. Chapin III, and P. W. Stackhouse Jr.
796 (2007), Climate-induced boreal forest change: Predictions versus current observations,
797 Global and Planetary Change 56, 274–296.
798 Stohl, A., E. Andrews, J. F. Burkhart, C. Forster,1 A. Herber, S. W. Hoch, D. Kowal, C.
799 Lunder, T. Mefford, J. A. Ogren, S. Sharma, N. Spichtinger, K. Stebel, R. Stone, J.
800 Strom, K. Tørseth, C. Wehrli, and K. E. Yttri (2006), Pan-Arctic enhancements of light
801 absorbing aerosol concentrations due to North American boreal forest fires during
802 summer 2004, *J. Geophys.,Res.*, Vol. 111, D22214, doi:10.1029/2006JD007216.
803 Stohl, A. (2006), Characteristics of atmospheric transport into the Arctic troposphere, *J.*
804 *Geophys. Res.*, *111*, D11306, doi:10.1029/2005JD006888.
805 Stone, R. S., G. Anderson, E. Andrews, E. Dutton, J. Harris, E. Shettle, A. Berk (2007),
806 Incursions and radiative impact of Asian dust in northern Alaska, *Geophys. Res. Lett.*,
807 Vol. 34, L14815, doi: 10.1029/2007/GL029878.
808 Stone, R. S., G. P.Anderson, E. P. Shettle, E. Andrews, K. Loukachine, E. G. Dutton, C.
809 Schaaf, and M. O. Roman III (2008), Radiative impact of boreal smoke in the Arctic:
810 Observed and modeled, *J. Geophys. Res.*, in press.
811 Turetsky, M., K. Wieder, L. Halsey, and D. Vitt (2002), Current disturbance and the
812 diminishing peatland carbon sink, *Geophys. Res. Lett.*, *29*(11), 1526,
813 doi:10.1029/2001GL014000.
814 Turquety, S., et al. (2007), Inventory of boreal fire emissions for North America in 2004:
815 Importance of peat burning and pyroconvective injection, *J. Geophys. Res.*, *112*,
816 D12S03, doi:10.1029/2006JD007281.

840

841 Figure 5. Remotely sensed fire counts for the Alaska region from the MODIS sensor on
842 the Terra satellite for the years 2002 through 2008.

843

844 Figure 6. Spectral Deconvolution Algorithm (SDA) computed daily average fine and
845 coarse mode AOD versus day of the year from June 1, 2004 through September 12, 2004
846 at Bonanza Creek, Alaska.

847

848 Figure 7. A comparison of the daily average 380-500 nm Angstrom exponents as a
849 function of 500 nm AOD for the Bonanza Creek data from 2004 versus the AERONET
850 data from the major tropical region biomass burning sites of ABRACOS Hill, Brazil
851 (2002 data; southern Amazonia) and Mongu, Zambia (2004; southern Africa savanna
852 burning region). For all three sites the data for the June through October biomass burning
853 seasons are shown.

854

855 Figure 8. Spectral Deconvolution Algorithm (SDA) computed daily average fine mode
856 fraction (FMF) for the Bonanza Creek site plotted versus $\alpha_{380\text{-}500}$ and compared with
857 measurements made in Brazil and Zambia (from the same observations as shown in
858 Figure 6).

859

860 Figure 9. Almucantar retrievals of a) aerosol volume size distributions b) single scattering
861 albedo, and c) imaginary part of the refractive index from the Bonanza Creek site in 2004
862 and 2005 for scans where AOD(440nm)>0.4. These averages are plotted as a function of

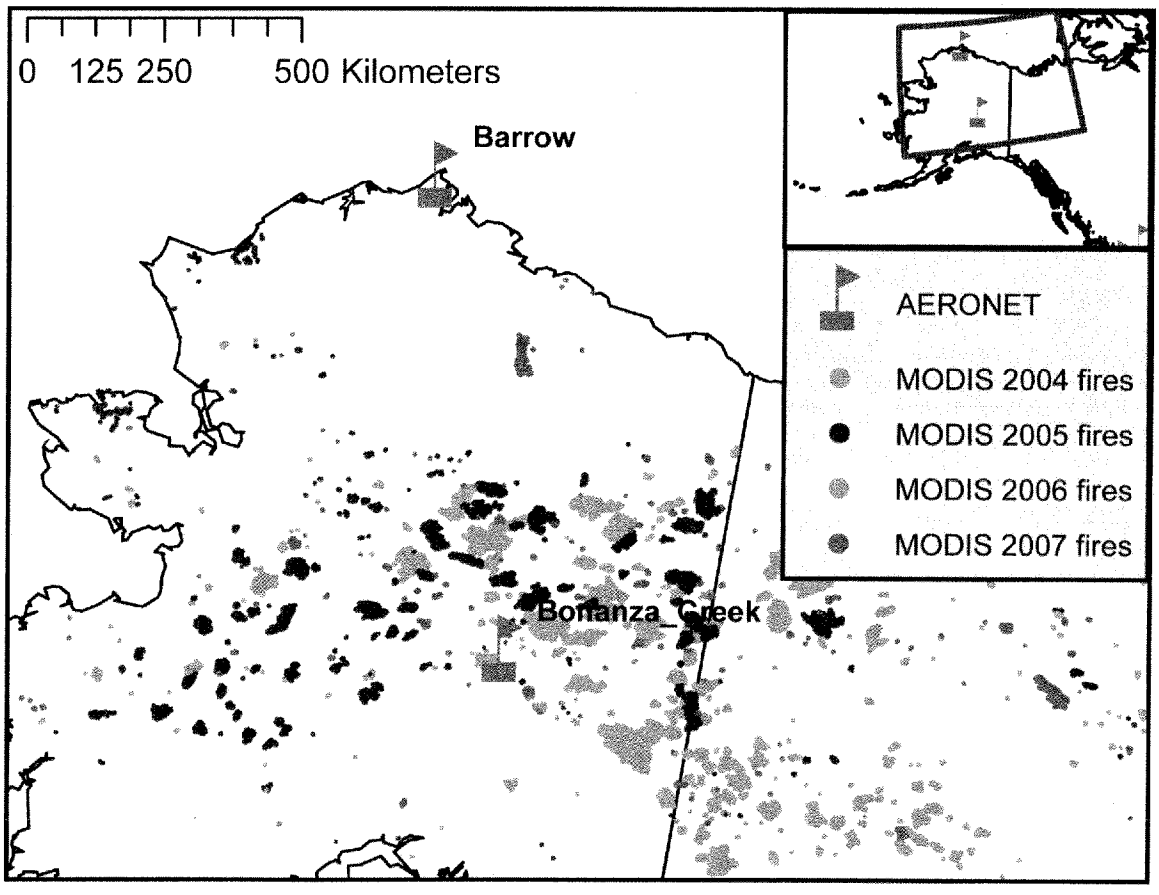
0 125 250 500 Kilometers
Barrow
Bonanza_Creek
AERONET
MODIS 2004 fires
MODIS 2005 fires
MODIS 2006 fires
MODIS 2007 fires

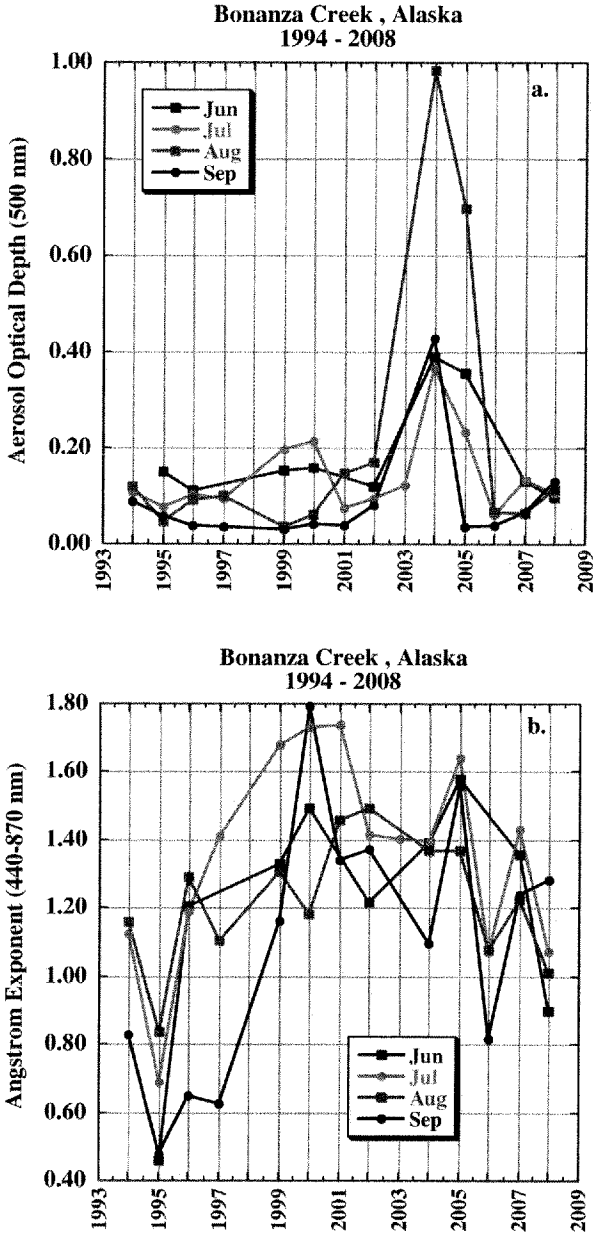

Figure 3. Time series of a) monthly average AOD at 500 nm and and b) Angstrom exponent (440-870 nm), by year for the summer and early fall months (June-September) at Bonanza Creek.

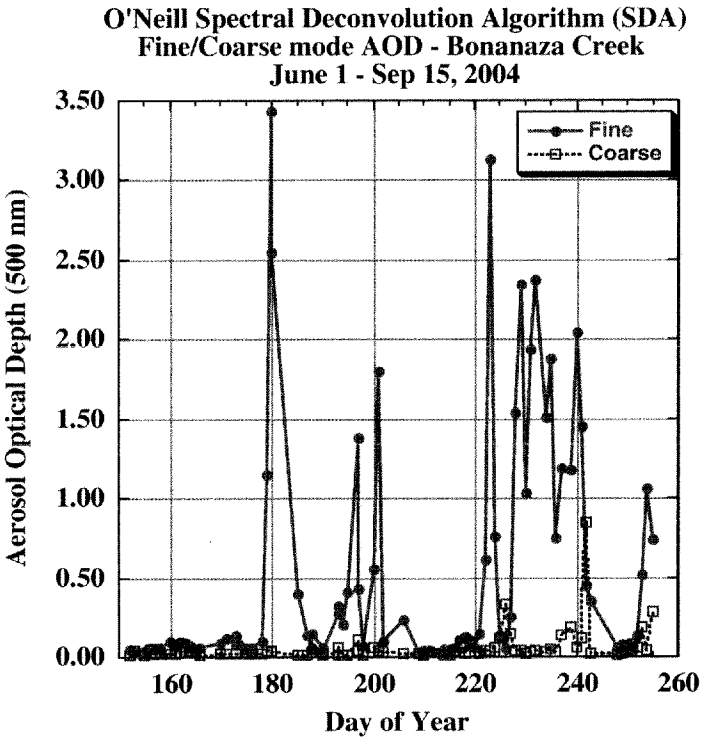

Figure 6. Spectral Deconvolution Algorithm (SDA) computed daily average fine and coarse mode AOD versus day of the year from June 1, 2004 through September 12, 2004 at Bonanza Creek, Alaska.

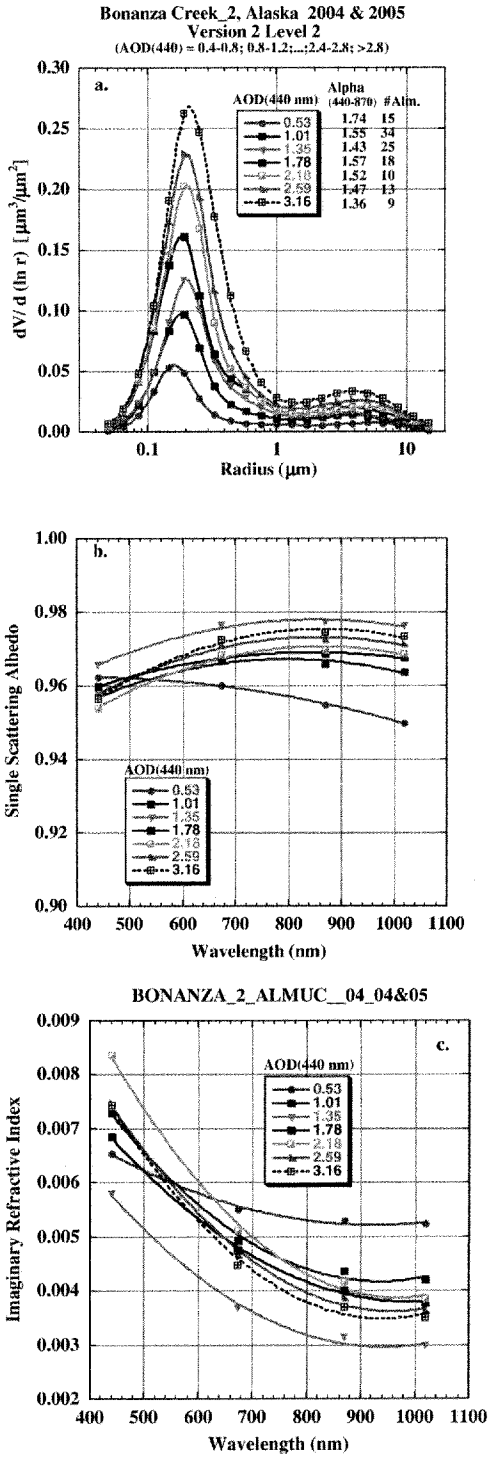

Figure 9. Almucantar retrievals of a) aerosol volume size distributions b) single scattering albedo, and c) imaginary part of the refractive index from the Bonanza Creek site in 2004 and 2005 for scans where AOD(440nm)>0.4. These averages are plotted as a function of AOD(440nm) for AOD bins from 0.4-0.8, >0.8-1.0,…,>2.4-2.8, >2.8 resulting in averages of from 9 to 35 almucantar scans per bin.

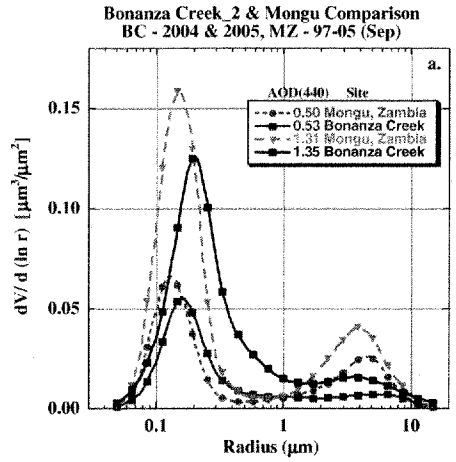

1046

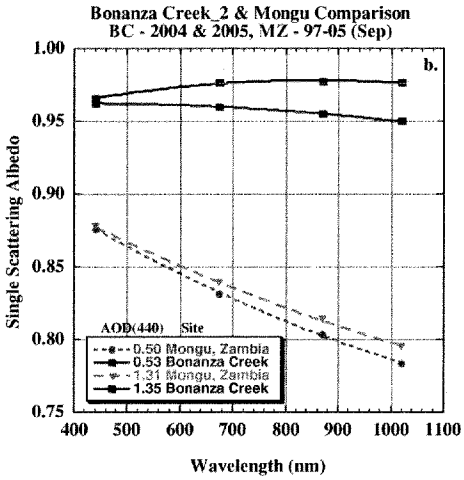

1047

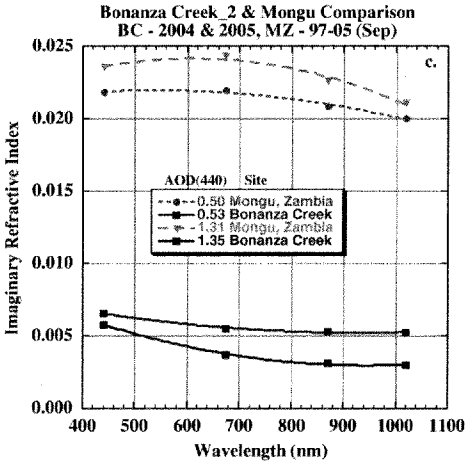

1048
1049
1050

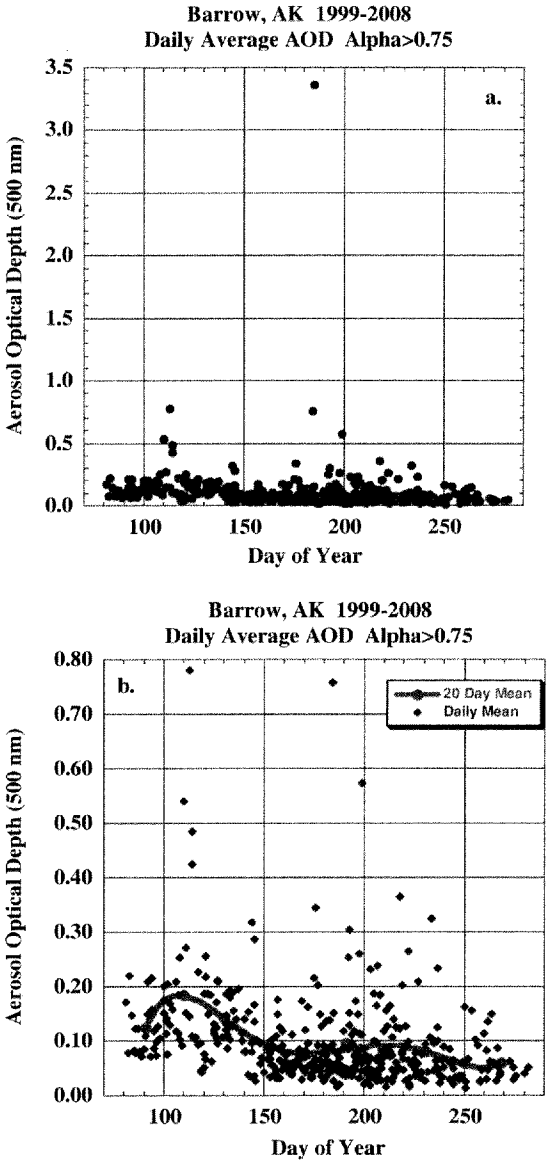

Figure 12. a) The daily average 500 nm AOD measured at the Barrow AERONET site as a function of the day of the year for all monitoring during the 1999 through 2008 time interval. b) The same as in a) but with the single outlier point of AOD (500 nm) of 3.4 from July 3, 2004 removed, and with 20 day averages computed.